Electronic Supplementary Material (ESI) for Polymer Chemistry.

Supporting Information

Interconnectivity and morphology control of poly-high internal phase emulsions under photo-polymerization

Subeen Kim,‡[1] Jongmin Q. Kim,‡[1] Siyoung Q. Choi,[1] and KyuHan Kim*[2]

[1] Department of Chemical and Biomolecular Engineering, Korea Advanced Institute of Science and Technology (KAIST), Republic of Korea

[2] Department of Chemical and Biomolecular Engineering, Seoul National University of Science and Technology (SeoulTech), Republic of Korea

* Corresponding Author: kyuhankim@seoultech.ac.kr

‡ Co-first Authors

Contents

Supplementary Materials and Methods

Maximum thickness measurement : Conical tubes containing 10.5 mL (height of 85 mm in 15 mL conical tube) of HIPEs with either surfactants or particles are photo-polymerized for 30 min under 1000 W-light. After removing the unreacted reagents, the solidified height of the polyHIPEs was measured using a steel ruler.

Dynamic light scattering (DLS) analysis : To measure the size distribution of the Al_2O_3 nanoparticles in the water phase, a dynamic light scattering analysis was conducted using a zetasizer nano ZS90 (Malvern). The aqueous dispersion of Al_2O_3 with 5 wt% was mixed at 3000 rpm for 1 minute (Vortex mixer, DAIHAN Scientific) and then sonicated for 1 hour (Ultra-sonic Cleaner Set, DAIHAN Scientific, 253 W). Before the measurement, the dispersion was diluted about 100 times with deionized water, and ~ 1 mL of the diluted dispersion was then analyzed at 25 °C.

Attenuated total reflectance Fourier transform infrared (ATR-FTIR) spectroscopy: ATR-FTIR spectroscopy was conducted using a Nicolet iS50 spectrometer (Thermo Fisher Scientific). The absorption spectra of samples were recorded in the mid-infrared region from 4000 to 400 cm^{-1}.

Differential scanning calorimetry (DSC) : Thermal characteristics of polyHIPEs were measured using a Netzsch DSC 204 F1 Phoenix (Netzsch-Geratebau GmbH). About 11 mg of the dried polyHIPE sample was placed in an aluminum crucible, and prior to the actual measurement, the first heating cycle was performed to 200 °C to remove the thermal history of the polymer matrix. The measurements were carried out in the temperature range of 25 to 200 °C with 10 K/min of heating rate under N_2 atmosphere, and the glass transition temperature (T_g) of each sample was determined by the inflection point of the heat flow change.

Pore size analysis : In order to determine the average diameter of voids and pore throats, more than 100 drops were analyzed for each polyHIPE sample using *ImageJ* program (NIH). Here, *ImageJ* program was also utilized to post-process the SEM images of the polyHIPEs (e.g., conversion of SEM images to binary images with appropriate threshold settings).

Uniaxial compression test: The compression tests of polyHIPEs were carried out using a custom-built universal testing machine with a 200 N load cell (DBCM-20, Bongshin Loadcell, South Korea). The compression tests were conducted at a compression rate of 0.5 mm/min with at least three pieces (~ 0.5 cm × 0.4 cm, ~ 3 mm-thickness) per each polyHIPE sample. Here, the compressional modulus of each sample was obtained by calculating an average slope of a stress-strain curve in the initial linear region where a linear correlation between stress and strain exists (a compressional strain ~ 10%). The yield stress of each sample was determined from the stress at the intersecting point of the extrapolation line of the initial linear slope and the straight line indicating the stress value at the plateau region.[1,2]

Comparison of the thickness of the photo-polymerized HIPE

According to the examination of the maximum thickness of each photo-polymerized HIPE, it is confirmed that the thicknesses of polyHIPEs stabilized by surfactants (Darocur 1173 : 28 mm, Irgacure 2959 : 17 mm, and LAP : 45 mm) are considerably greater than those of particle-stabilized HIPEs (Darocur 1173 : 21 mm, Irgacure 2959 : 10 mm, and LAP : 32 mm), regardless of the type of initiators (Figure S1a). The shorter thicknesses of Pickering polyHIPEs can be attributed to the nanoparticle aggregates located at the oil-water interface or in the aqueous phase because the intensity average diameter (~ 412 nm, Figure S1b) of particle aggregates measured by DLS is comparable to the wavelength (250 – 370 nm) of UV-visible light absorbed by photo-initiators. Accordingly, the scattering can occur significantly inside the Pickering HIPEs during polymerization, which hampers light to penetrate into the bottom of the sample, thereby strongly indicating that the lower the intensity of light reaching the bottom of the sample, the shorter the thickness of polyHIPE.

Additionally, it turns out that the type of photo-initiator has a significant influence on the maximum height of the monolith, as shown in Figure S1. In particular, the monoliths samples prepared by LAP are the thickest, whereas the samples with Irgacure 2959 are the thinnest, and this significant difference in the thickness is probably due to the light intensity in the range of wavelength where each photo-initiator can absorb. According to the spectrum of light intensity of a 1000 W-metal halide lamp, the light intensity is significantly decreased as the wavelength decreases from 365 nm to 250 nm. In fact, the wavelength where a maximum absorbance of LAP occurs is about 360 nm, thereby strongly suggesting that photo-polymerization of HIPEs with LAP can be effectively promoted under the light irradiation of the l000W- lamp. On the other hand, D1173 and I2959 have optimal absorption wavelengths at about 290 nm and 260 nm, respectively, and in this range, the light intensity of metal halide lamps is considerably lower than that of LAP. Therefore, as the wavelength where the optimal absorption occurs decreases from 360 nm, the maximum height of the polyHIPE monolith decreases as well, which is in descending order of LAP (45 mm), D1173 (28 mm), and LAP (17 mm).

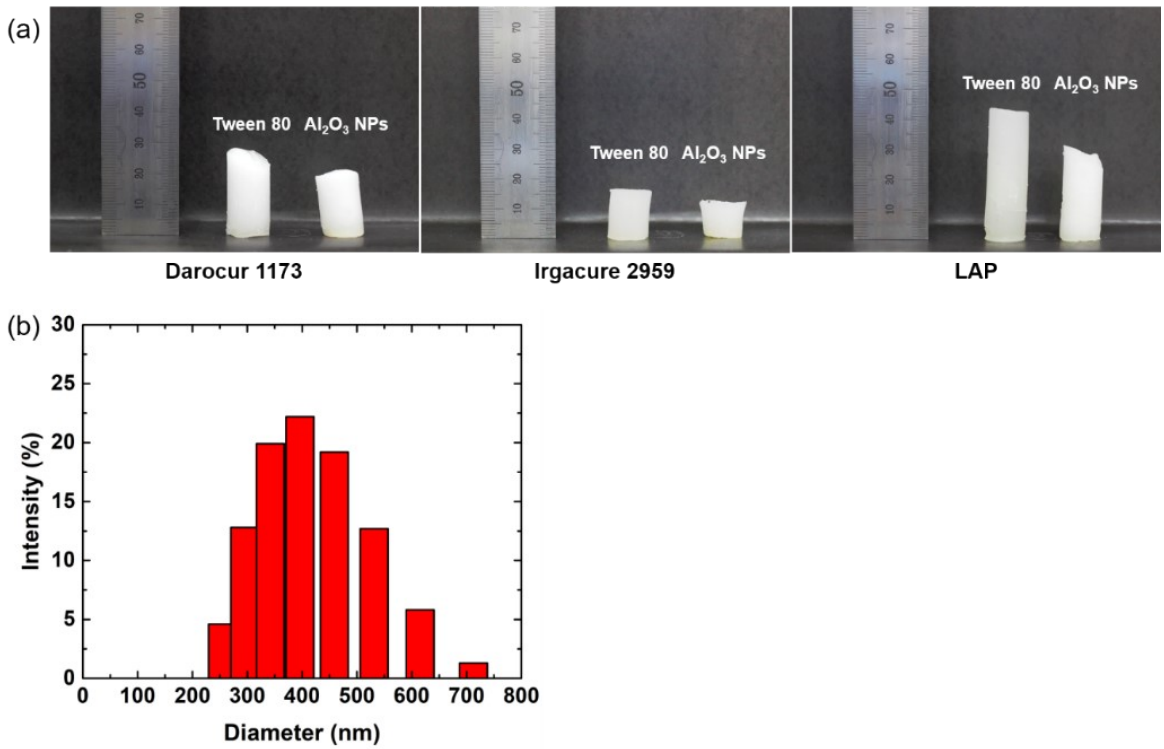

Figure S1. (a) The maximum height of photo-polymerized HIPEs under 1000 W light with different emulsifiers and photo-initiators. (b) The size distribution of aggregates of Al_2O_3 nanoparticles measured by the DLS technique.

ATR-FTIR spectra for the PolyHIPEs and the water phases

In order to confirm that photo-polymerization of HIPE has been successfully completed, FTIR spectra of the resulting polyHIPE were investigated using the attenuated total reflectance (ATR) technique. In particular, the ATR-FTIR analysis was performed on the samples before and after polymerization. The PolyHIPEs were analyzed in the dried state while for the samples before polymerization, only the aqueous phase in the HIPEs was analyzed because acrylic acid (AA) and N,N'-methylenebisacrylamide (MBAm), i.e., monomer and cross-linker, are mostly located in the water phase.

As shown in Figure S2a, the presence of both AA and MBAm in the aqueous aliquot of the HIPE containing Tween 80 and D1173 (a solid burgundy line) is well proven by IR analysis because both AA and MBAm molecules have vinyl groups. Specifically, the peak at 984 cm^{-1} can be assigned to the out-of-plane C-H bending vibration of mono-substituted alkene, and this strongly suggests that vinyl monomer and vinal cross-linker exit in the water phase. Furthermore, the peaks at 1635 cm^{-1} and 1616 cm^{-1} and the peak at 1690 cm^{-1} correspond to C=C stretch and carbonyl stretch, respectively, and these are also strong evidence for the presence of AA and MBAm.[3] However, the O-H bond for AA and the N-H bond for MBAm cannot be identified due to the broadened peak from 3000 cm^{-1} to 3700 cm^{-1} stemming from the O-H bending of water.

On the other hand, it is noteworthy that the chemical bonds incorporated in the polyHIPE monolith (a solid red and a solid pink line in Figure S2a) can be dramatically changed compared to chemical bonds in the aqueous phase. For example, the peaks of sp3 C-H stretch[4] at 2956 cm^{-1}, 2924 cm^{-1}, and 2855 cm^{-1} evolves while the magnitude of vinyl peaks at 984, 1616, and 1635 cm^{-1} are significantly decreased. This result implies that the vinyl group of monomers undergoes radical polymerization. In addition, the magnitude of carbonyl peak at 1701 cm^{-1} is much greater than other peaks, and this strongly indicates that the monolith is entirely composed of acrylic matrix with a small amount of surfactant and photo-initiator. The magnitude of the peak above 3000 cm^{-1} (a solid burgundy line in Figure S2a) considerably decreases owing to water removal through the drying process, and the remaining absorbance is presumably due to the presence of O-H bond and N-H bond originated from the residues of AA and MBAm.

Using different photo-initiators and emulsifiers, FTIR spectra were also investigated, and as a result, similar spectral changes are seen when other photo-initiators (Irgacure 2959 (Figure S2b) and LAP (Figure S2c)) or another emulsifier (Al2O3 (Figure S3)) are utilized. Comparing the IR spectra of the monolith with that of the aqueous phase, the peak intensities of the C=C bond (1610-1640 cm^{-1}) and sp2 C-H bond (980 cm^{-1}) decrease in all cases, whereas the peak intensities for the sp3 C-C bond (2850-2960 cm-^{1}) and C=O bonds (1700-1710 cm-1) significantly increase. This can be the result of the conversion of vinyl monomers to the formation of C-C bonds between the monomer units. In summary, these results strongly indicate that the photo-polymerization of acrylic acid and MBAm to polymeric monoliths proceeds successfully with all types of photo-initiators and emulsifiers.

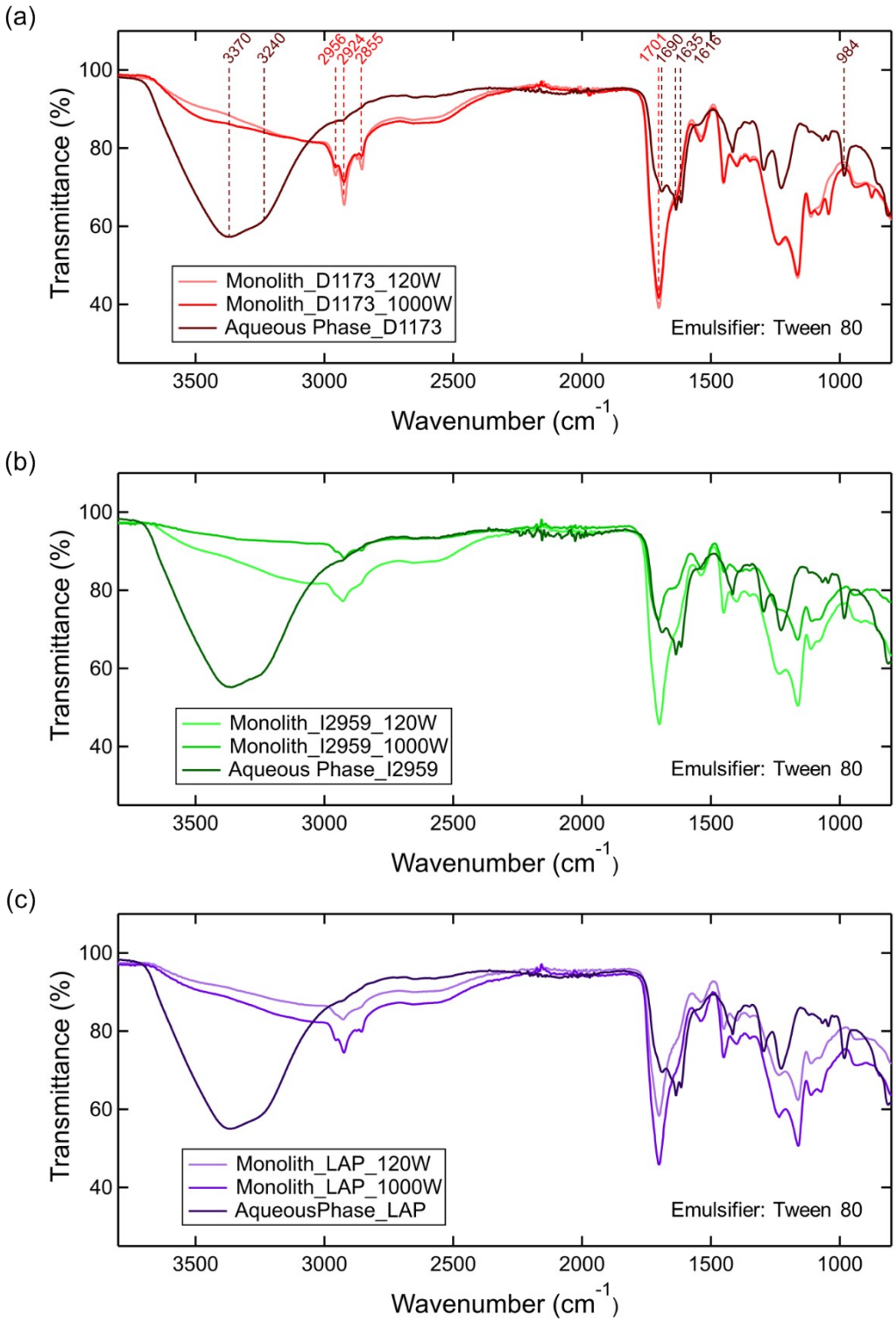

Figure S2. The graph for FTIR spectra of photo-polymerized HIPEs with Tween80 surfactants. The HIPEs are polymerized by three different photo-initiators: (a) Darocur 1173, (b) Irgacure 2959, and (c) LAP under 120 and 1000 W of light intensity. Each graph also includes the FTIR spectrum for the aqueous phase containing the same surfactant and initiators.

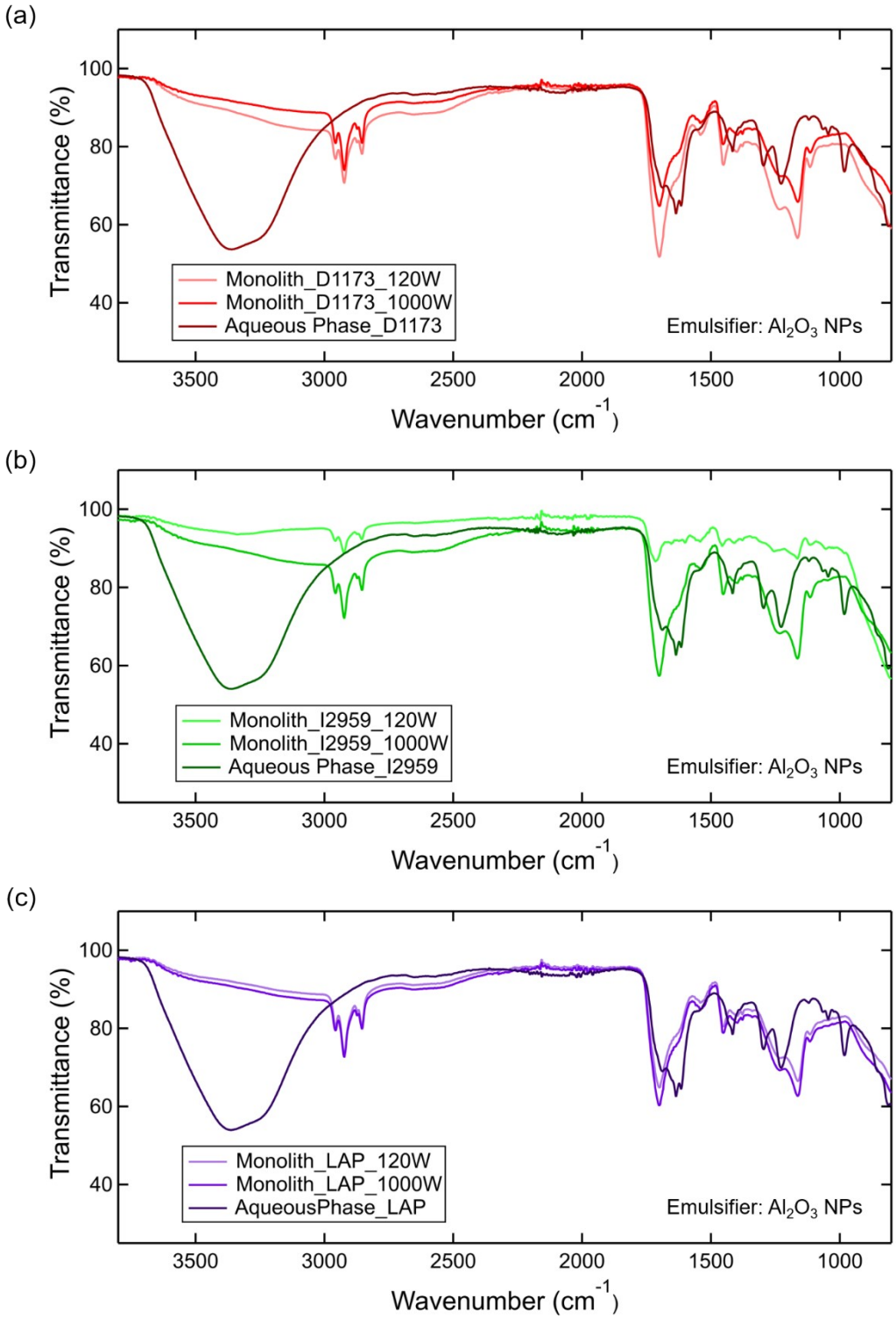

Figure S3. The graph for FTIR spectra of photo-polymerized HIPEs with Al_2O_3 nanoparticles. The HIPEs are polymerized by three different photo-initiators: (a) Darocur 1173, (b) Irgacure 2959, and (c) LAP under 120 and 1000 W of light intensity. Each graph also includes the FTIR spectrum for the aqueous phase containing the same particle and initiator.

DSC thermograms for the PolyHIPEs

To analyze the thermal properties of poly(acrylic acid) (PAA)-based polyHIPEs, DSC measurements for the polyHIPEs were conducted here. As shown in Figure S4, T_g of polyHIPE with D1173 (indicated in a solid black line) was observed at about 127 °C, which is significantly greater than 102 ~ 109 °C of poly(acrylic acid) (PAA) homopolymer.[5–7] This might be occurred due to the restricted mobility of chain segments by the crosslinking of PAA as well as the formation of anhydride during the initial heating treatment to 200 °C.[5] Furthermore, in order to investigate the effect of the presence of pore throats on the T_g values, T_gs of the PolyHIPEs with different initiators are measured and compared each other. As a result, it is successfully confirmed that T_g values of polyHIPEs are almost identical, regardless of the presence of the pore throats.

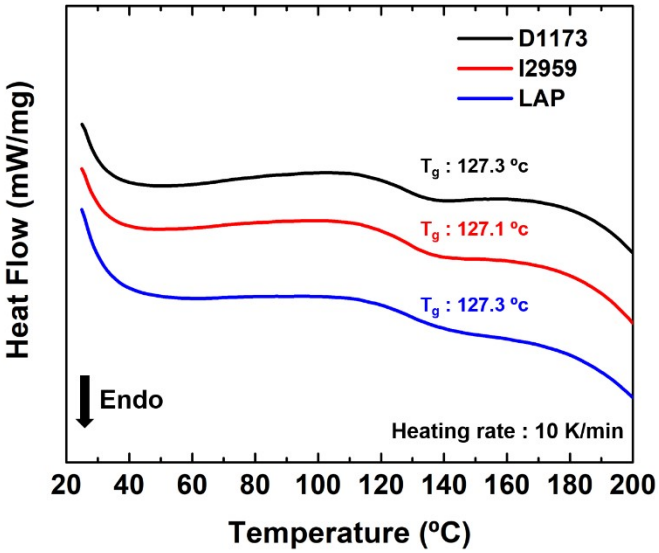

Figure S4. DSC thermograms of polyHIPEs after the 1st heating to 200 °C. Here, each polyHIPEs with TWEEN80 were photo-polymerized under a 120 W of light intensity in the presence of D1173 (solid black line), I2959 (solid red line), and LAP (solid blue line).

Pore size analysis for the PolyHIPEs

Table S1. The diameter of voids and pore throats of polyHIPEs, depending on the type of emulsifiers and photo-initiators, and the intensity of light.

Experimental Conditions			Diameter of Voids and Pore Throat		
Emulsifier	**Initiator**	**Light Power**	**Number average Diameter of Voids**	**Volume average Diameter of Voids**	**Number average Diameter of Pore Throat**
Tween80	D1173	120 W	2.43 ± 1.07 μm	3.91 μm	-
Tween80	I2959	120 W	2.98 ± 1.29 μm	4.60 μm	-
Tween80	LAP	120 W	2.62 ± 1.42 μm	5.17 μm	0.55 ± 0.30 μm
Tween80	D1173	1000 W	2.45 ± 1.30 μm	4.37 μm	0.82 ± 0.47 μm
Tween80	I2959	1000 W	2.41 ± 1.27 μm	4.77 μm	0.68 ± 0.34 μm
Tween80	LAP	1000 W	2.50 ± 1.24 μm	4.35 μm	0.56 ± 0.33 μm
Al_2O_3	D1173	120 W	124.7 ± 30.3 μm	145.7 μm	-
Al_2O_3	I2959	120 W	116.1 ± 25.3 μm	131.4 μm	-
Al_2O_3	LAP	120 W	76.8 ± 31.2 μm	116.4 μm	-
Al_2O_3	D1173	1000 W	79.7 ± 36.8 μm	118.7 μm	-
Al_2O_3	I2959	1000 W	46.0 ± 20.8 μm	76.1 μm	-
Al_2O_3	LAP	1000 W	69.2 ± 34.7 μm	132.5 μm	-

As shown in Table S1, for surfactant-stabilized HIPEs, a number average diameter and a volume average diameter of voids turn out to be about 2.5 μm and about 5 μm, respectively. In the previous literatures for the porous polymeric materials, the volume average diameter had been more frequently utilized compared to the number average diameter,[8–10] so that here, the average value primarily refers to the volume average one. In addition, a number average diameter of pore throats is also measured, and it gives 0.6 - 0.8 μm. Interestingly, the size of pore throat using D1173 and I2959 seems to be greater than that of LAP, although the number of pore throats of them is much less than that of LAP, as shown in Figure 4. This might be attributed to the uniformity of polymer film thickness where pore throats can be formed. When hydrophobic photo-initiators (D1173 and I2959) are utilized, the film rupture can occur throughout the entire film, as shown in Figure S5a. In contrast, for polyHIPE synthesized with LAP, only the thinnest part of the polymer film can be ruptured, which generates a small pore throat (Figure S5b). For particle-stabilized HIPEs, the volume average diameter of voids is about 100 μm, which is over 20 times greater than that of surfactant-stabilized ones.

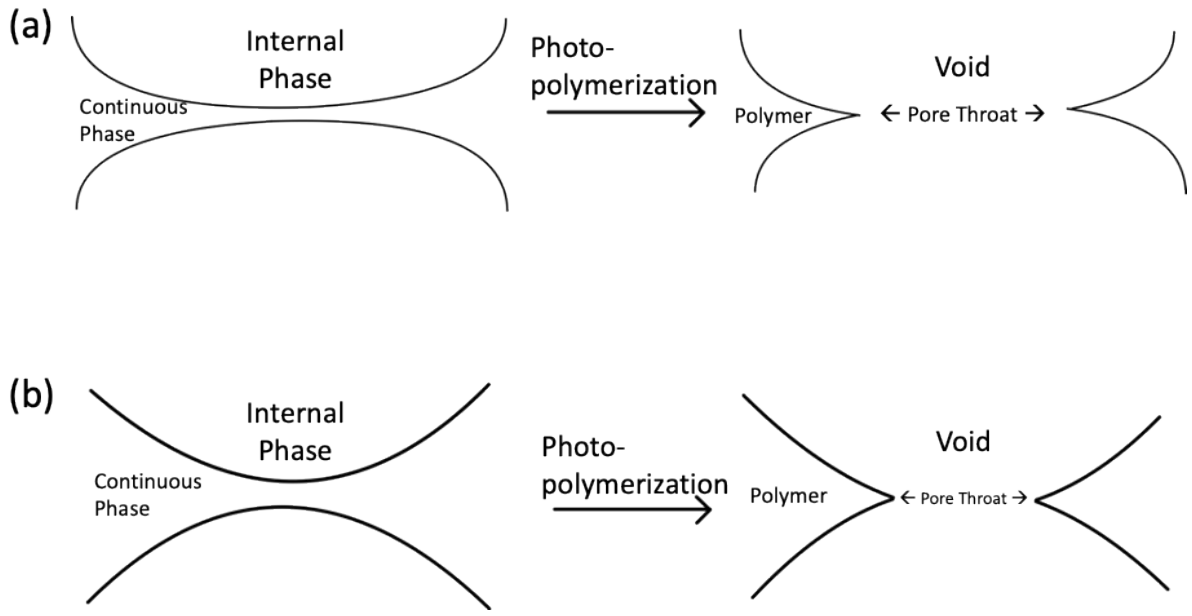

Figure S5. (a) The scheme depicting the pore throat formation via the thin film formation using D1173. (b) The scheme depicting the pore throat formation via the thick film formation using LAP.

Comparison of compressional properties of polyHIPEs

In order to compare the compression properties of polyHIPEs with and without interconnectivity, compression tests of polyHIPEs were conducted by a custom-built compression machine. The tests were conducted with closed-pore polyHIPE samples prepared by Darocur 1173 under 120 W-light, which were stabilized with either Tween 80 or Al_2O_3 particles. In addition, for the polyHIPE with an open-pore structure, the compressional properties of samples prepared by Darocur 1173 under 1000 W-light with Tween 80 were measured to evaluate the effect of interconnectivity. Compressional moduli of each sample were obtained from stress-strain curves recorded with a constant compression rate of 0.5 mm/min.

As shown in Figure S6a, all the graphs indicate an initial linear region, a plateau region, and a bulk compression region under continuous compression.[1] For compressional modulus, the surfactant stabilized-polyHIPE with closed-pores indicates the largest value while the surfactant stabilized-polyHIPE with open-pores shows the lowest value (Figure S6a and Table S2), showing 4.57 MPa, and 2.85 MPa, respectively. This possibly occurs due to the different strength of the polymeric walls in each polyHIPE. For example, in the polyHIPEs with closed pores, the wall between pores can be fully occupied by polymer matrix, and this matrix can effectively store energy during the compression. On the other hand, for polyHIPE with pore throats, the wall has many empty holes that give rise to the interconnection between pores, thereby resulting that the wall can be easily deformable under compression. Therefore, polyHIPE with closed-pores shows a greater compressional modulus than that of one with open-pores.

In the presence of colloidal particles in the polymer wall, it can be expected to achieve a significantly high modulus due to the rigid structure of the particle layer and the thick film thickness. However, as shown in Figure S6, polyHIPE with Al_2O_3 nanoparticles shows a lower compression modulus (3.07 MPa) than that of the surfactant-stabilized one. This may be because the polyHIPE with Al_2O_3 nanoparticles has a much greater pore size (~ 100 μm) than that of surfactant-stabilized one (~ 5 μm), as indicated in Table S1. The total surface area of the polymer film can be roughly proportional to ~ d^2, where d is the diameter of pores, so that compared to the surfactant-stabilized polyHIPE, the much smaller surface area of the particle-stabilized polyHIPE can be expected. Furthermore, this lower surface area can provide a lower energy store capacity, thereby resulting in the slightly lower compressional modulus, even though the polyHIPE with particles can have a greater stiffness of the polymer film than the surfactant-stabilized one.

In addition, the yield stresses for each polyHIPE are also measured, based on the stress-strain curve (Figure S6b). Interestingly, the yield stresses (1.09 Mpa and 1.69 MPa for the HIPEs with open pores and closed pores, respectively) for the HIPEs with surfactants is considerably greater than that (0.85 Mpa) of the HIPEs with nanoparticles. This seems to occur due to the brittle characteristic of the particle-embedded polymer walls and relatively flexible characteristic of the surfactant-stabilized polymer walls. Specifically, it has been known that the brittle wall can contain a relatively low yield strain and low yield stress[11] with a

considerably long plateau region where the slope is almost zero. On the other hands, the flexible wall can contain the greater yield stress and yield strain, compared to those from the brittle one, and it also indicates a relatively short plateau region with a small value of slope. Accordingly, our results are well agreed with those mentioned above.

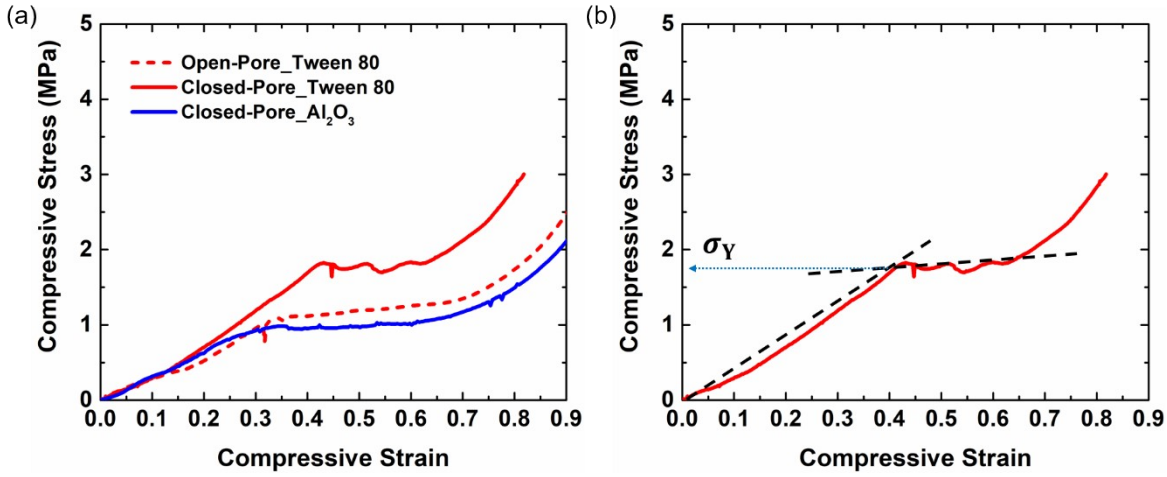

Figure S6. The results of the compression test for polyHIPEs with D1173: a) stress-strain curves for three different polyHIPE samples. b) The way to obtain the yield stress from the intersection of the extrapolation line of the initial slope and the stress line in a plateau region.

Table S2. Compressional moduli and yield stresses of polyHIPEs, depending on the presence of interconnectivity and the type of emulsifiers.

Samples	Compressive Modulus, E[a)]	Yield Stress, σ_y [b)]
Open-pore_Tween 80	2.85 ± 0.48 MPa	1.09 ± 0.12 MPa
Closed-pore_Tween 80	4.57 ± 1.14 MPa	1.69 ± 0.37 MPa
Closed-pore_ Al_2O_3	3.07 ± 1.00 MPa	0.85 ± 0.14 MPa

[a)]Compressional moduli were obtained from the initial strain region of 0.1; [b)]the collapse stresses were taken from the way, shown Figure S6b. E and σ_y were obtained from at least 3 samples.

Supplementary References

1 L. J. Gibson and M. F. Ashby, Mechanics of Three-Dimensional Cellular Materials., *Proc. R. Soc. London, Ser. A Math. Phys. Sci.*, 1982, **382**, 43–59.

2 L. Gibson and M. Ashby, *Cellular Solids*, 1988.

3 L. Feng, H. Yang, X. Dong, H. Lei and D. Chen, pH-sensitive polymeric particles as smart carriers for rebar inhibitors delivery in alkaline condition, *J. Appl. Polym. Sci.*, 2018, **135**, 1–9.

4 T. Wan, Q. Chen, Q. Zhao, R. Huang, L. Liao, J. Xiong and L. Tang, Synthesis and swelling properties of a pH-and temperature-dual responsive hydrogel by inverse microemulsion polymerization, *J. Appl. Polym. Sci.*, 2015, **132**, 1–8.

5 J. J. Maurer, D. J. Eustace and C. T. Ratcliffe, Thermal Characterization of Poly (acrylic acid), 1987, 196–202.

6 A. R. Greenberg and Kusy R.P., Influence of crosslinking on the glass transition of poly(acrylic acid), *J. Appl. Polym. Sci.*, 1980, **25**, 1785–1788.

7 A. Eisenberg, T. Yokoyama and E. Sambalido, Dehydration kinetics and glass transition of poly(acrylic acid), *J. Polym. Sci. Part A-1 Polym. Chem.*, 1969, **7**, 1717–1728.

8 B. P. Binks and C. P. Whitby, Silica Particle-Stabilized Emulsions of Silicone Oil and Water: Aspects of Emulsification, *Langmuir*, 2004, **20**, 1130–1137.

9 D. Georgieva, V. Schmitt, F. Leal-Calderon and D. Langevin, On the possible role of surface elasticity in emulsion stability, *Langmuir*, 2009, **25**, 5565–5573.

10 K. Reinheimer, M. Grosso, F. Hetzel, J. Kübel and M. Wilhelm, Fourier Transform Rheology as an innovative morphological characterization technique for the emulsion volume average radius and its distribution, *J. Colloid Interface Sci.*, 2012, **380**, 201–212.

11 K. C. Rusch, Load-compression behavior of brittle foams, *J. Appl. Polym. Sci.*, 1970, **14**, 1263–1276.